



## Investigation of the synthesis of a grinding intensifier from secondary raw materials and its influence on the microstructural development of cement stone

Ristavletov R.A. <sup>1</sup> , Auyesbekova M.A. <sup>1</sup> , Karimov M.U. <sup>2</sup> , Kambarov M.A. \* <sup>1</sup> ,  
Kasimova G.A. <sup>3</sup> , Kudabayev R.B. <sup>1</sup> , Bektursunova A.K. <sup>1</sup> , Artykova Zh.K. <sup>1</sup> 

<sup>1</sup> South-Kazakhstan University named after M. Auevov, Kazakhstan,

<sup>2</sup> Tashkent Research Institute of Chemical Technology, Uzbekistan,

<sup>3</sup> Tashkent Institute of Architecture and Civil Engineering, Uzbekistan

**Abstract.** This paper presents data on the synthesis of cement grinding intensifiers produced from oil and gas processing wastes, namely secondary alkanolamines. The results of physicochemical characterization of the raw materials are reported, including the optimal purification conditions for the wastes and the synthesis parameters of the grinding intensifiers, as well as the physicochemical properties of the obtained products. It was found that the optimal conditions for producing the grinding intensifier involve conducting the reaction at 45°C for 6 hours with a 1:9 component ratio. The effects of the synthesized intensifiers on the cement clinker grinding process were investigated, including their influence on particle size distribution and the mineralogical composition of modified cements. The particles of the modified cement were shown to exhibit a predominantly spherical morphology; the maximum laser diffraction value reached 13.5%, the intensity was 88%, and the particle size was mainly around 2 μm (more than 53.5%), while the fraction of particles within the 100-200 μm range was 4.87%. X-ray diffraction and differential thermal analysis revealed that hydration of the modified cement is accompanied by a slight decrease in the diffraction intensity of calcium silicate phases (C<sub>2</sub>S and C<sub>3</sub>S), whereas an increase in the diffraction intensity of calcium hydroxide (Ca(OH)<sub>2</sub>) was observed. This indicates the formation of calcium hydroxide and calcium silicate hydrate (C-S-H) during cement hydration. The diffraction peaks of these phases were detected within the ranges of 30-33° 2θ and 40-45° 2θ. In addition, the presence of aluminates (C<sub>3</sub>A) and ferrite (C<sub>4</sub>AF) phases within 40-45° 2θ corresponds to calcium carbonate (CaCO<sub>3</sub>) observed in low-intensity regions between 29.4° 2θ and 48.5° 2θ, which is associated with CO<sub>2</sub> absorption from the atmosphere. These changes reflect phase transformations during hydration and the formation of phases that are critical for strength development. The optimal dosage of the grinding intensifier in the cement composition was determined to be 0.02 wt.% (based on dry residue).

**Keywords:** cement grinding intensifiers, energy efficiency improvement, cement stone, secondary alkanolamines, particle size distribution, physicochemical analysis

\*Corresponding author E-mail: [medet\\_2030@mail.ru](mailto:medet_2030@mail.ru)

**Please cite this article as:** Ristavletov R.A., Auyesbekova M.A., Karimov M.U., Kambarov M.A., Kasimova G.A., Kudabayev R.B., Bektursunova A.K., Artykova Zh.K. Investigation of the synthesis of a grinding intensifier from secondary raw materials and its influence on the microstructural development of cement stone. Construction Materials and Products. 2026. 9 (1). 9. DOI: 10.58224/2618-7183-2026-9-1-9

---

## 1. INTRODUCTION

Cement is a key construction material used in buildings and infrastructure, and its global production has already exceeded 4 billion tons per year [1]. As the third largest industrial energy consumer, the cement industry accounts for approximately 7% of industrial energy consumption and is responsible for about 7% of global CO<sub>2</sub> emissions [2]. In the context of global sustainable development, cement manufacturing faces major challenges related to energy conservation and reduction of CO<sub>2</sub> emissions. The use of supplementary cementitious materials (SCMs), such as fly ash, blast furnace slag, phosphorus slag, calcined clay, etc., in the production of blended (composite) cements makes it possible to reduce the clinker factor and is considered one of the effective approaches to address this problem [3-5]. However, a major drawback of these substitutes is the slow early strength development of composite cements [6, 7]. Consequently, some cement producers have shifted toward finer clinker grinding, in particular to increase the fraction of cement particles smaller than 3 μm, which are critical for achieving high strength within the first 24 hours of cement hydration [3]. Nevertheless, clinker grinding accounts for approximately 30-40% of the electricity consumed in cement production. Therefore, the development of cement grinding intensifiers (GIs) derived from industrial wastes is an important research task, as it can enhance the energy efficiency of cement production and contribute to improving the environmental situation in the region.

Cement grinding intensifiers include high-molecular-weight surfactants (HMW surfactants) and their salts with various metals [6, 8]. According to the international classification adopted at the 3<sup>rd</sup> International Congress on High-Molecular-Weight Surfactants and approved by the International Organization for Standardization (ISO) in 1960, HMW surfactants are organic compounds that contain one or more polar functional groups and dissociate in aqueous solutions to form long-chain anions exhibiting surface activity [9,10].

The so-called hydrophilic-lipophilic balance (HLB) index characterizes the ratio of polar and nonpolar functional groups within a surfactant molecule. The group numbers of hydrophilic (polar) groups are considered positive (heat is released), whereas those of hydrophobic (lipophilic) groups are negative (heat is absorbed). Surfactants containing the SO<sub>3</sub><sup>-</sup> functional group include widely used compounds such as sodium lignosulfonates and polymethylenephthalenesulfonates (superplasticizer C-3) [10-12]. Surfactants containing the COO<sup>-</sup> functional group include fourth-generation plasticizers – polycarboxylates. Polycarboxylates are comb-shaped polymers and are also referred to as hyperplasticizers [13-15].

At present, grinding intensifiers based on amines, glycols, and carboxylic acids are widely applied [16, 17]. Prziwara et al. [18] emphasized that amine-based intensifiers outperform glycol-based ones in preventing particle agglomeration. Similar conclusions were reported by Mishra et al. [16]. A number of studies have also confirmed the effectiveness of GI dosage in relation to the fresh-state properties of cementitious systems [17, 19, 20]. San et al. [13] demonstrated that there exists an optimal GI dosage from the standpoint of energy efficiency. The authors noted that energy efficiency increases with increasing GI dosage up to a certain level, after which it decreases as dosage continues to rise. In addition, the GI dosage rate is an important factor for admixture compatibility in systems with reduced cement and water content.

Grinding intensifiers are added during clinker comminution to reduce electrostatic forces and minimize agglomeration of clinker grains [16]. Their chemical composition includes alkanolamines such as triethanolamine (TEA), triisopropanolamine (TIPA), and diethanolisopropanolamine (DEIPA), as well as glycols such as propylene glycol (PG), monoethylene glycol (MEG), and diethylene glycol (DEG). Polycarboxylate ethers (PCEs) are also widely used as grinding additives. Due to their organic

polar nature, grinding intensifiers are preferentially adsorbed on surfaces formed by the rupture of electrovalent bonds such as Ca-O and Si-O, which reduces surface energy forces [16]. This reduction allows higher cement fineness to be achieved at a given energy input [16-18]. Mishra et al. quantitatively showed that the primary effect of grinding intensifiers is the reduction of agglomeration energy [19]. More recently, it has been demonstrated that such additives can also improve the particle separation process in ground clays [10].

It is well known that alkanolamines influence cement hydration in addition to improving grinding performance [20-22]. TEA and TIPA have been used as setting accelerators and strength enhancers [23, 24]. Ramachandran observed that TEA may retard alite hydration, while significantly accelerating the reaction of C<sub>3</sub>A and the formation of ettringite [24, 25]. Moreover, TEA may affect the solubility of fly ash [26]. TIPA has been reported to enhance strength at later ages [27, 28]. DEIPA can promote ettringite formation and accelerate hydration of aluminat clinker phases [29, 30].

A review of the literature indicates that the influence of grinding intensifiers on cement manufacturing processes and on certain fresh and hardened properties of cement-based systems has been investigated. However, there remains limited information regarding the effects of GI type and dosage on the rheological behavior and hardened-state performance of cementitious systems. In addition, data on the influence of GI presence and dosage on cement compatibility with polycarboxylate-based admixtures (PCEs) are scarce. Due to the large number of interacting parameters, the mechanism of GI action has not yet been fully clarified. The lack of information on these issues complicates the selection of practical GI dosages from a broader performance and compatibility perspective.

## 2. METHODS AND MATERIALS

Polyacrylonitrile (PAN), oil and gas processing wastes from PetroKazakhstan Oil Products LLP (secondary monoethanolamine (MEA), diethanolamine (DEA), and triethanolamine (TEA)), an 8 wt.% sodium hydroxide solution, methanol, and hydrochloric acid were used as raw materials for the synthesis of cement grinding intensifiers.

To synthesize GI-PAN (grinding intensifier obtained via polyacrylonitrile hydrolysis), 10 g of PAN, 220 mL of 8 wt.% NaOH solution, and 500 mL of methanol were used.

In a 500 mL round-bottom flask equipped with a reflux condenser, 220 mL (0.44 mol) of 8 wt.% NaOH solution was added, followed by 20 g (0.5 mol) of finely ground polyacrylonitrile. The mixture was heated in an oil bath to boiling (bath temperature approximately 100-110°C) and maintained for about 13 h. After the solution became colorless and transparent, heating was stopped, and the solution was cooled and transferred into a 500 mL beaker. Neutralization was performed using 0.5 N hydrochloric acid to pH 8.0-8.2 (universal indicator).

Sodium polyacrylate was precipitated from the solution by adding 150 mL of methanol. The resulting precipitate was filtered using a Büchner funnel and washed with methanol until chloride traces disappeared in the filtrate. The purified sodium polyacrylate was air-dried for 48 h. The polymer yield was 31.2 g. Sodium polyacrylate is a white powder soluble in water and melts with decomposition.

Free polyacrylic acid was obtained by acidifying a 5 wt.% aqueous solution of sodium polyacrylate with an equivalent amount of 10 wt. % hydrochloric acid. The precipitated polyacrylic acid was washed with water until chloride traces disappeared in the mother liquor, followed by air-drying for 48 h.

Physicochemical characterization of the raw materials and the synthesized grinding intensifiers was performed using FTIR spectroscopy, chromatography, and mass spectrometry, while the physicochemical and chemical properties of the synthesized intensifiers were evaluated using standard methods. The particle size distribution of the modified cement was determined using a Bettersizer S3 Plus laser particle size analyzer (Bettersize Instruments Ltd., China). The mineralogical composition of cement and cement stone was determined by X-ray diffraction (XRD), differential thermal analysis (DTA), and electron microscopy.

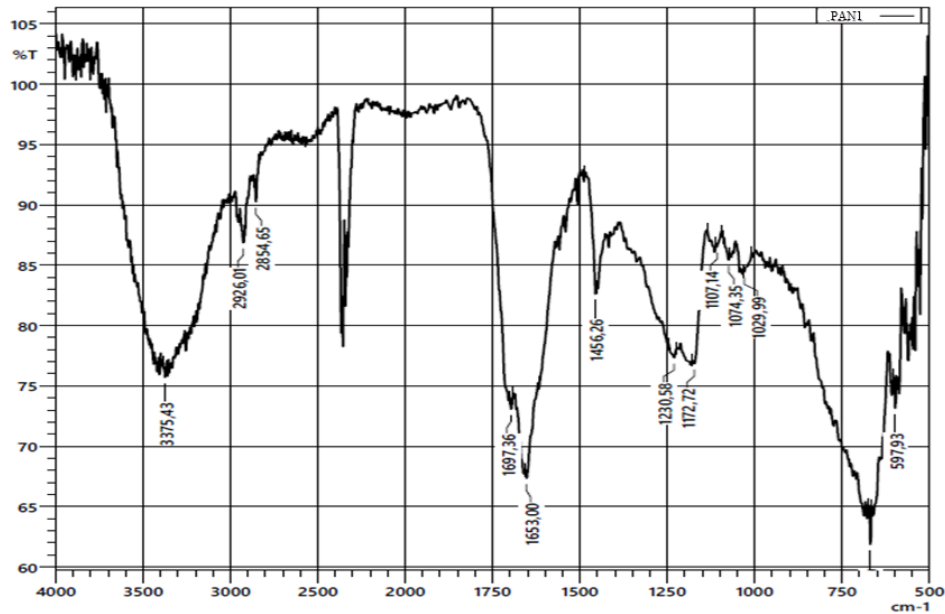


**Fig. 1.** FTIR spectra of GI-PAN.

As shown in Fig. 1, the spectrum exhibits two strong carbonyl absorption bands at  $1697\text{ cm}^{-1}$  and  $1653\text{ cm}^{-1}$ . These peaks indicate the simultaneous presence of a carboxylic acid group ( $1697\text{ cm}^{-1}$ ) and an amide group ( $1653\text{ cm}^{-1}$ ), suggesting that the compound contains both acidic and amide functionalities within a single molecule.

A broad band at  $3375\text{ cm}^{-1}$  is typically attributed to O-H stretching vibrations (characteristic of carboxyl groups) or N-H stretching vibrations. If assigned to N-H stretching, this further supports the presence of amide groups.

The absorption bands at  $2926\text{ cm}^{-1}$  and  $2854\text{ cm}^{-1}$  correspond to the stretching vibrations of methylene ( $\text{CH}_2$ ) groups, whereas the peak at  $1456\text{ cm}^{-1}$  is associated with their bending vibrations. This indicates the presence of a long carbon chain or an aliphatic component.

The pronounced peaks at  $1697\text{ cm}^{-1}$  ( $\text{C}=\text{O}$ ) and in the range of  $1230\text{--}1172\text{ cm}^{-1}$  ( $\text{C}-\text{O}$ ) provide clear evidence of carboxylic acid functional groups.

Regeneration procedure for methyldiethanolamine. Spent methyldiethanolamine is commonly used for  $\text{CO}_2$  and  $\text{H}_2\text{S}$  capture in natural gas processing; therefore, secondary methyldiethanolamine contains absorbed acidic gases. To remove these gases, the secondary methyldiethanolamine is first filtered and then passed through a fixed-bed activated carbon column. After activated carbon treatment, the methyldiethanolamine is further purified using cation- and anion-exchange resins. For this purpose, the cation exchanger KU 2-8 is pre-treated by soaking in a 3 wt.% hydrochloric acid solution for 24 h, while the anion exchanger AN-31 is soaked in a 5 wt.% alkali solution for 24 h. Subsequently, the activated-carbon-treated methyldiethanolamine is passed sequentially through the cation-exchange and anion-exchange resins. As a result, the color of the treated methyldiethanolamine becomes significantly lighter, indicating effective purification.

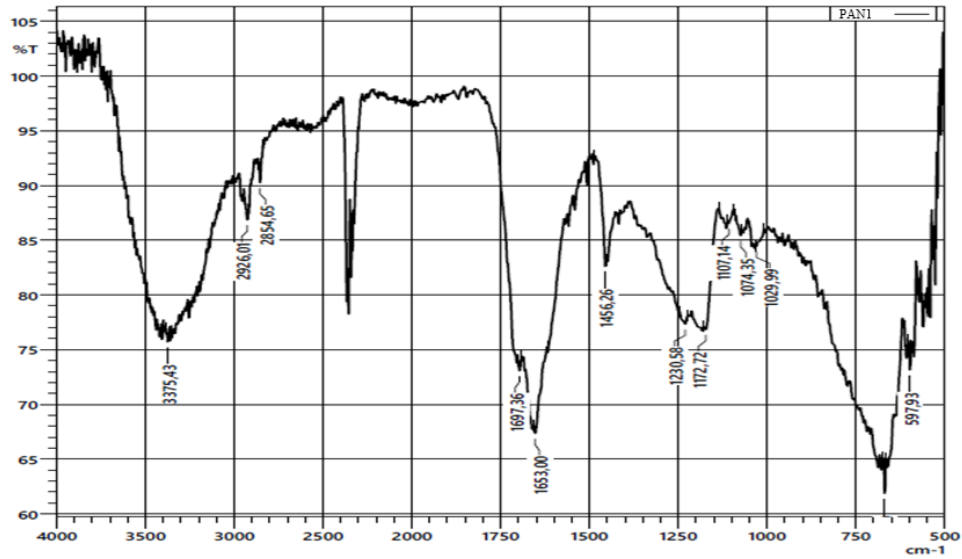


Fig. 2. FTIR spectra of purified methyldiethanolamine.

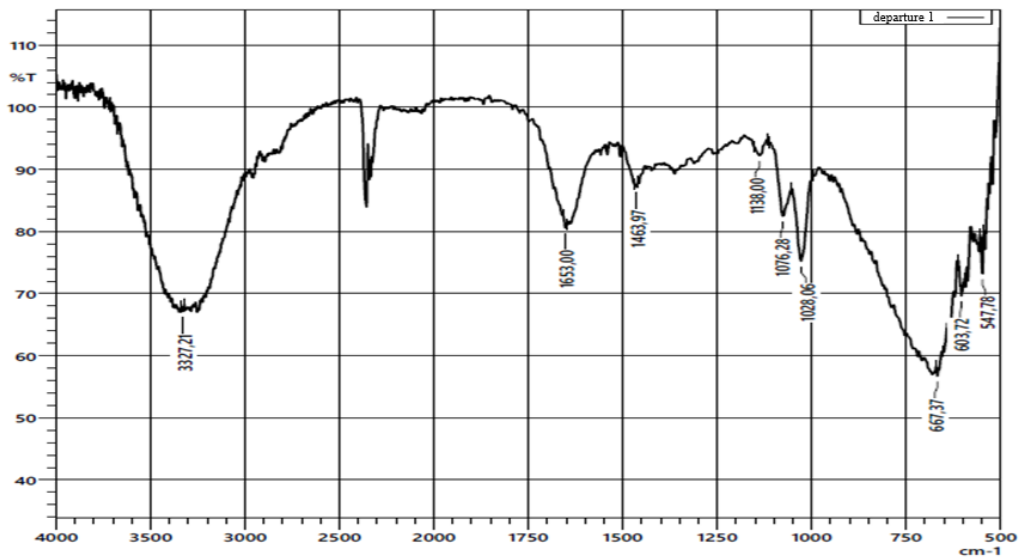


Fig. 3. FTIR spectra of unpurified MDEA.

A comparison of the FTIR spectra of purified and unpurified methyldiethanolamine (MDEA) revealed the following features:

- Purified MDEA: no C=O absorption band is observed; a broad  $\nu(\text{OH})$  band appears within 3600-3000  $\text{cm}^{-1}$ ; C-H stretching vibrations are detected in the range of 2970-2870  $\text{cm}^{-1}$ ; strong absorption bands attributed to C-O/C-N stretching vibrations are observed within 1260-1000  $\text{cm}^{-1}$ .

- Waste MDEA (saturated with  $\text{CO}_2$  and  $\text{H}_2\text{S}$ ):

- Bicarbonate/carbonate species (from  $\text{CO}_2$  absorption): distinct intensity increase around ~1650-1600  $\text{cm}^{-1}$ , ~1360-1380  $\text{cm}^{-1}$ , and ~1010-1040  $\text{cm}^{-1}$ .

- Hydrosulfide/ $\text{H}_2\text{S}$ -related species: the appearance of a new band or a sharp increase in intensity of the S-H stretching band at ~2550-2570  $\text{cm}^{-1}$ ; in addition, broad N- $\text{H}^+$ -related bands may increase within 3000-2600  $\text{cm}^{-1}$  and ~1550-1480  $\text{cm}^{-1}$ .

The  $\nu(\text{OH})$  absorption band becomes broader and shifts toward lower wavenumbers, which can be attributed to increased protonation and the formation of an extended hydrogen-bond network.

Synthesis of the grinding intensifier based on hydrolyzed sodium polyacrylate and methyldiethanolamine. The grinding intensifier based on hydrolyzed sodium polyacrylate (from PAN hydrolysis) and methyldiethanolamine was synthesized in a 5 L reactor, into which the calculated amount of hydrolyzed polyacrylonitrile was charged. The mixture temperature was increased to 50°C, after which the calculated amount of methyldiethanolamine was added slowly over 1 h. The reaction mass was then cooled to room temperature. Unreacted methyldiethanolamine was separated from the cooled reaction mass by vacuum distillation. The obtained product was a viscous liquid with a color varying from light yellow to orange.

Temperature plays a key role in the production of the grinding intensifier. The figure below shows the dependence of the intensifier yield on the reaction temperature. Three different initial reactant ratios were evaluated.

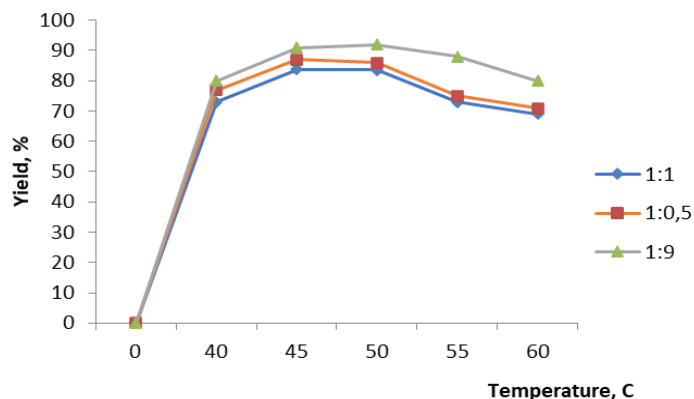


**Fig. 4.** Effect of reaction temperature on grinding intensifier yield. The molar ratios of hydrolyzed polyacrylonitrile to methyldiethanolamine were as follows: (1) 1:1; (2) 1:0.5; (3) 1:9.

As shown in Fig. 4, the optimal component ratio for grinding intensifier synthesis is 1:9, and the optimal reaction temperature is 45°C. Under these conditions, the intensifier yield reaches 92%. The highest yield is achieved at the initial reactant ratio of 1:9; however, the performance (or quality) of the resulting intensifiers is relatively low. Therefore, an optimal synthesis temperature of 45°C was selected for producing the grinding intensifier.

In the production of chemical products, reaction time also plays a significant role. To determine the optimal reaction conditions (in terms of yield), three initial reactant ratios were also considered.

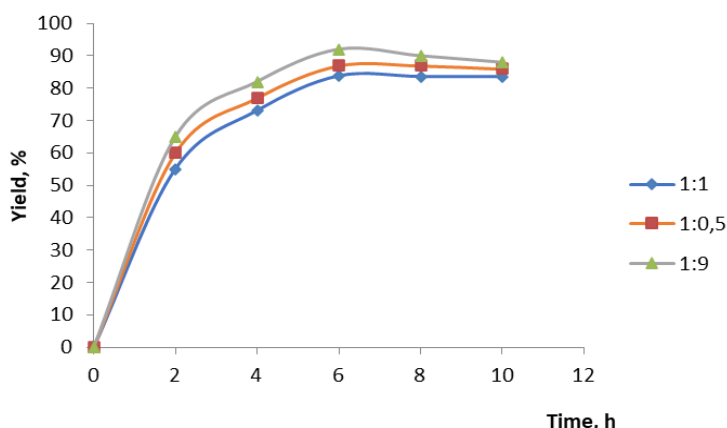


**Fig. 5.** Effect of reaction time on grinding intensifier yield. The molar ratios of hydrolyzed polyacrylonitrile to diethanolamine were as follows: (1) 1:1; (2) 1:0.5; (3) 1:9.

As shown in Fig. 5, a 92% yield of the grinding intensifier is achieved when the reaction is performed under the optimal conditions for 6 h. Further prolongation of the reaction under the same conditions results in a decrease in yield. This is attributed to the intensification of side reactions (such as crosslinking, decomposition, intermolecular interactions, etc.), which reduce the functional efficiency of the grinding intensifier.

Thus, the optimal conditions for grinding intensifier synthesis are a reaction temperature of 45°C, a reaction time of 6 h, and a component ratio of 1:9. The product obtained under these conditions demonstrates a very high performance.

**Table 1.** Physicochemical properties of the grinding intensifiers.

Parameter	Value
Appearance	Liquid with a reddish tint
Density at 20°C, not less than	1.2
Water content, wt.%, not more than	3.0
Hydrogen ion activity (pH) of a 2.5 wt.% aqueous solution	9.0 ± 1.0
Chloride ion content in dry matter, wt.%, not more than	0.001
Water solubility at 20°C, g/100 g water	22

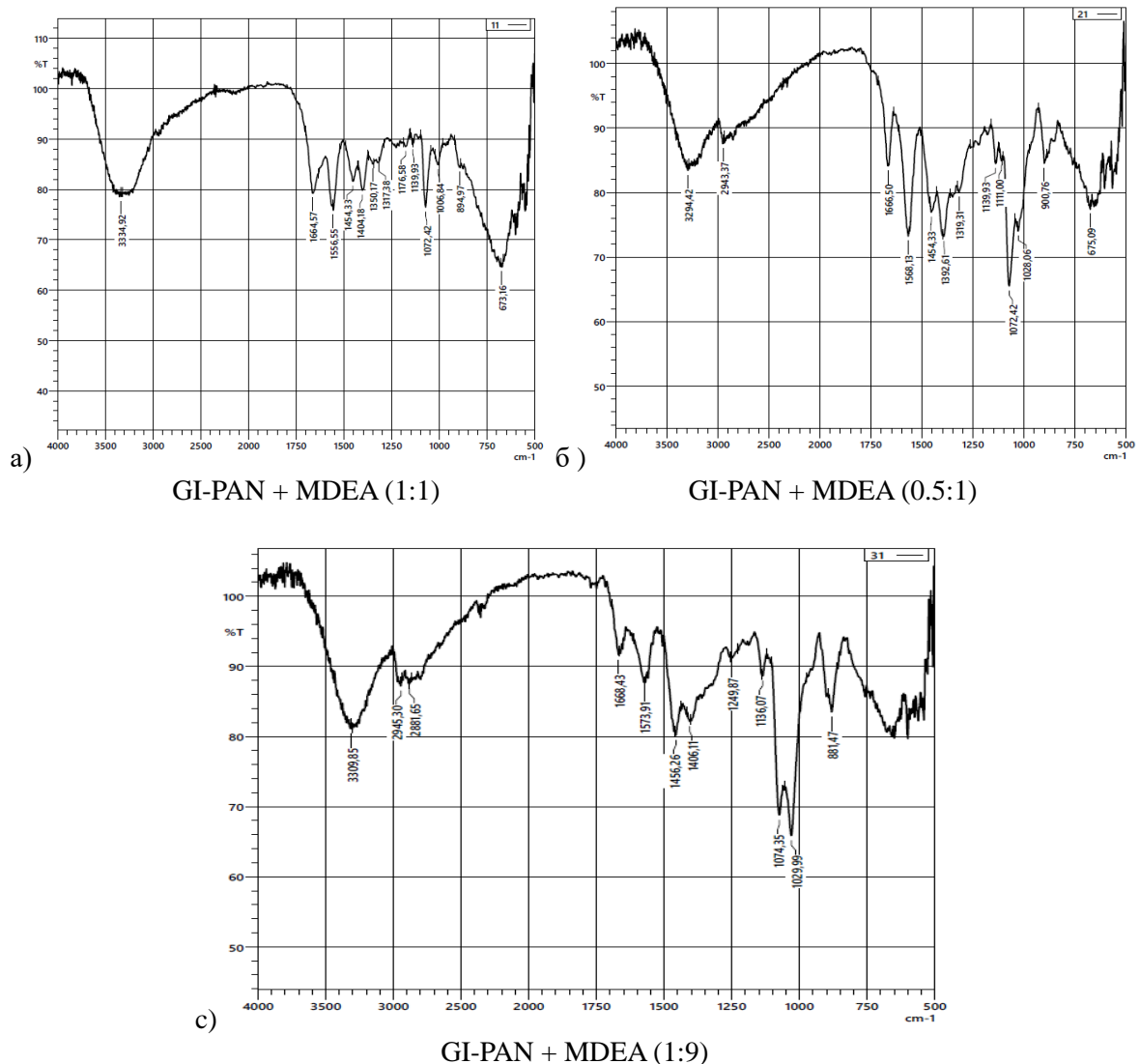


**Fig. 6.** FTIR spectra of GI-PAN + MDEA at the ratios: (A) 1:1, (B) 0.5:1, and (C) 1:9.

FTIR spectroscopy results indicate that GI-PAN, depending on the degree of hydrolysis, contains residual  $\text{C}\equiv\text{N}$  groups as well as amide ( $\text{CONH}_2/\text{CONH}$ ), carboxyl ( $\text{COOH}/\text{COO}^-$ ), and  $\text{OH}$  functional groups. Methyl-diethanolamine (MDEA), in turn, is a tertiary amine capable of forming a protonated ammonium species ( $\text{R}_3\text{NH}^+$ ), thereby shifting the  $\text{COOH} \leftrightarrow \text{COO}^-$  equilibrium toward the formation of carboxylate-ammonium salt pairs. With increasing MDEA content, the broad absorption band in the  $3600\text{--}3000\text{ cm}^{-1}$  region becomes wider and its maximum shifts to lower wavenumbers, which is indicative of stronger hydrogen bonding. In the  $2970\text{--}2870\text{ cm}^{-1}$  region, corresponding to C-H stretching vibrations, the intensity slightly increases as the MDEA fraction increases. A band at  $\sim 1715\text{--}1730\text{ cm}^{-1}$  is associated with free  $\text{COOH}$  ( $\text{C}=\text{O}$ ) groups, whereas the region of  $\sim 1680\text{--}1645\text{ cm}^{-1}$  corresponds to amide I vibrations. In GI-PAN-MDEA systems, the  $1715\text{--}1730\text{ cm}^{-1}$  band decreases with increasing  $\text{COO}^-$  content (carboxylate formation), while the amide I band remains present depending on the hydrolysis degree. Carboxylate formation is supported by the appearance/intensification of characteristic  $\text{COO}^-$  bands at  $\sim 1570\text{--}1610\text{ cm}^{-1}$  ( $\nu_{\text{asym}}$ ) and  $\sim 1390\text{--}1415\text{ cm}^{-1}$  ( $\nu_{\text{sym}}$ ). When ammonium-carboxylate pairs are formed,  $\nu_{\text{asym}}$  may shift upward while  $\nu_{\text{sym}}$  slightly shifts downward, leading to an increase in  $\Delta\nu = \nu_{\text{asym}} - \nu_{\text{sym}}$ , which indicates an increased ionic character of bonding.

At the 0.5:1 ratio, free  $\text{COOH}$  groups are expected to be almost completely neutralized; therefore, the  $1715\text{--}1730\text{ cm}^{-1}$  band becomes very weak, whereas the  $\text{COO}^-$  pair ( $\nu_{\text{asym}} \sim 1570\text{--}1610\text{ cm}^{-1}$  and  $\nu_{\text{sym}} \sim 1390\text{--}1415\text{ cm}^{-1}$ ) appears sharp and intense. An increased  $\Delta\nu$  (typically within  $160\text{--}230\text{ cm}^{-1}$ ) suggests a higher contribution of ionic ammonium-carboxylate interactions. The  $\text{OH}/\text{NH}$  region ( $3600\text{--}3000\text{ cm}^{-1}$ ) becomes strongly broadened and shifts downward due to a dense hydrogen-bonding network. If residual nitrile groups ( $\text{C}\equiv\text{N} \sim 2240\text{ cm}^{-1}$ ) are detected, their intensity is low, which implies a sufficiently high degree of PAN hydrolysis.

For the 1:1 system:

- the remaining free  $\text{COOH}$  fraction is minor; however, absorption bands in the  $1715\text{--}1730\text{ cm}^{-1}$  range may still be observed, suggesting incomplete conversion of carboxyl groups into ionic form;
- $\text{COO}^-$  bands remain distinct but slightly less intense than in the 0.5:1 system, and  $\Delta\nu$  may be somewhat lower;
- the  $3600\text{--}3000\text{ cm}^{-1}$  region remains broad but is shifted to slightly higher frequencies than for 0.5:1, indicating comparatively weaker hydrogen bonding;
- the  $\text{C}\equiv\text{N}$  band intensity is low-to-moderate, suggesting a high but not maximal hydrolysis/neutralization level compared with the 0.5:1 ratio.

In the 1:9 system (GI-PAN:MDEA):

- neutralization is limited; therefore, the  $\text{COOH}$  peak in the  $1715\text{--}1730\text{ cm}^{-1}$  region is preserved (in some cases a pronounced band may appear near  $1735\text{ cm}^{-1}$ );
- the  $\text{COO}^-$  peaks are present but less intense, and  $\Delta\nu$  is smaller due to a reduced fraction of ionic pairs;
- the  $3600\text{--}3000\text{ cm}^{-1}$  region shows higher-frequency absorption and reduced broadening, indicating weaker hydrogen bonding as fewer carboxylate-ammonium salts are formed due to low MDEA content;
- the  $\text{C}\equiv\text{N} \sim 2240\text{ cm}^{-1}$  band is relatively pronounced, implying a somewhat lower degree of hydrolysis/neutralization.

It should be noted that MDEA does not form amide bonds directly because it is a tertiary amine; however, it can deprotonate  $\text{COOH}$  groups, producing  $\text{COO}^-$ , while protonated MDEA forms ionic pairs ( $\text{R}_3\text{NH}^+\dots\text{COO}^-$ ). This is evidenced by a reduction in  $\nu(\text{C}=\text{O})(\text{COOH})$  and an increase in  $\nu_{\text{asym}}/\nu_{\text{sym}}(\text{COO}^-)$  bands. The conversion of residual nitrile groups in GI-PAN into amides during hydrolysis, followed by carboxyl formation, is reflected by decreasing intensity of  $\text{C}\equiv\text{N}$  ( $\approx 2240\text{ cm}^{-1}$ ), strengthening of amide I/II bands ( $\approx 1650/1550\text{ cm}^{-1}$ ), and increasing carboxylate bands ( $\approx 1570\text{--}1610/\approx 1390\text{--}1415\text{ cm}^{-1}$ ). The hydrogen-bonding structure (GI-PAN  $\text{OH}/\text{NH} \leftrightarrow \text{MDEA} - \text{OH}/\text{protonated amine}$ ) governs the broad absorption features in the  $3600\text{--}3000\text{ cm}^{-1}$  region; increasing MDEA strengthens the hydrogen-bond network, broadens the bands, and shifts them to lower frequencies.

Overall, the 0.5:1 ratio is characterized by the near-complete suppression of free  $\text{COOH}$ , strong  $\text{COO}^-$  bands, increased  $\Delta\nu$ , and extensive carboxylate-ammonium salt formation with a pronounced

hydrogen-bond network. The 1:1 ratio corresponds to a transitional state, with moderate neutralization and intermediate hydrogen bonding. The 1:9 ratio retains a noticeable  $-\text{COOH}$  peak, weaker  $\text{COO}^-$  features, smaller  $\Delta\nu$ , and relatively weaker hydrogen bonding, while the  $-\text{C}\equiv\text{N}$  band is more evident, indicating a lower extent of hydrolysis/neutralization.

### 3. RESULTS AND DISCUSSION

The synthesized grinding intensifier was used for grinding clinker samples (specific gravity 3.15) supplied by Shymkent cement plant “Standardcement”. Grinding was performed in a ball mill using a laboratory-scale ball mill with a standard ball charge of approximately 20 kg.

To evaluate the performance of grinding intensifiers in the laboratory ball mill, the initial feed material was required to have a particle size below 3.35 mm. Therefore, the clinker samples were предварительно crushed using a cone crusher until 100% of the particles passed 3.35 mm.

The particle size and particle size distribution of both unmodified cement and the modified product were determined. Measurements were carried out using a Bettersizer S3 Plus laser particle size analyzer (Bettersize Instruments Ltd., China). The Bettersizer S3 Plus measures particle sizes in the range of 0.01-3500  $\mu\text{m}$  and provides particle size distribution data. The instrument determines particle size automatically. By reducing the incidence angle using dual-focus technology, the convergence error of the dual-beam system is minimized, the observation angle is increased, and high sensitivity, accuracy, and efficiency are achieved. Automated image analysis provides information on particle morphology and enables correlation between particle size distribution and particle shape. Automatic refractive index measurement allows the selection of appropriate optical parameters for subsequent measurements.

The particle size characteristics of the modified cement were investigated, and the obtained results are presented in Fig. 7.

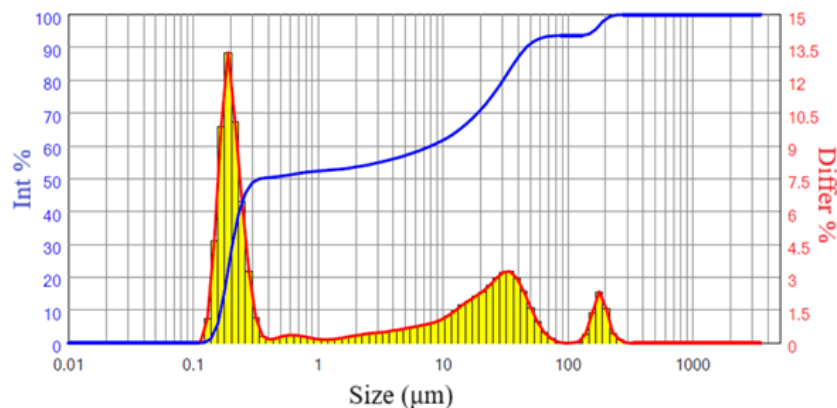


**Fig. 7.** Particle size and particle size distribution of the modified cement.

The obtained results indicate that particle size determination using the Bettersizer S3 Plus further increased the reliability of the analysis and confirmed the measured characteristics of the modified cement. The particles of the modified cement exhibited a predominantly spherical morphology. The maximum laser diffraction value was 13.5%, the intensity reached 88%, and the particle size was mainly around 2  $\mu\text{m}$ , accounting for more than 53.5% of the total fraction. The content of particles in the 100-200  $\mu\text{m}$  range was 4.87%.

The modified cement particles identified during the analysis were spherical and showed a predominantly amorphous structure, which was additionally confirmed by X-ray diffraction (XRD) analysis. In contrast, the investigation of unmodified cement particles demonstrated an increase in particle size. The corresponding results are presented in Figure 8. The particle size distribution of the unmodified cement was determined using the laser diffraction method. According to the results, particles with sizes up to 2  $\mu\text{m}$  accounted for 35.11% of the total composition, with a laser diffraction value of 5.5% and an intensity of 55%. At the same time, the fraction of particles within the 100-200  $\mu\text{m}$  range was 32.39%, with a laser diffraction value of 7.5% and an intensity of 73%.

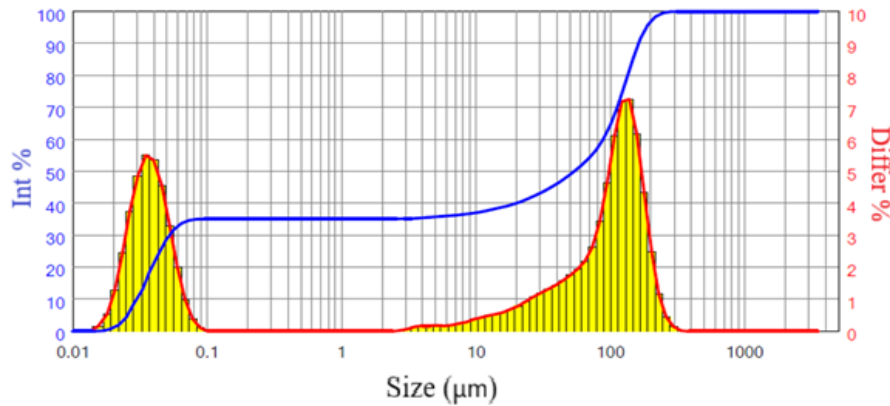


**Fig. 8.** Particle size and particle size distribution of the unmodified cement.

It was determined that the fraction of unmodified cement particles with sizes up to 2 µm is 35.11%, while the fraction of particles within the 100–200 µm range is 32.39%. All experiments conducted in this study are interrelated and form a comprehensive framework that provides a scientific and practical basis for using modified cement particles in the cement industry to improve the strength of concrete products.

The effect of the synthesized grinding intensifiers on the cement system was investigated, and it was found that certain performance characteristics of the obtained intensifiers exceed those of conventional grinding aids.

The results illustrating the influence of grinding intensifier dosage on cement stone strength over time are presented in Table 2.

**Table 2.** Dependence of cement stone strength on grinding intensifier dosage.

№	Additive dosage (wt.% of cement)	Cement stone strength, R (MPa)				
		1 day	3 days	7 days	14 days	28 days
1	Control sample	16.7	24.7	31.6	36.2	38.8
2	0.02	20.6	29.8	35.2	39.8	46.5
3	0.04	18.4	26.2	32.8	39.3	44.5
4	0.06	18.1	26.5	32.2	39.2	43.2
5	0.08	18.0	26.5	32.5	39.2	43.0
6	0.1	17.5	23.5	33.3	37.8	42.5

As can be seen from Table 2, the best performance was achieved at an additive dosage of 0.02 wt.% (based on dry residue). Under this dosage, the strength values increased consistently from 1 day up to 28 days, reaching a maximum of 46.5 MPa at 28 days. Although strength increased over time for all dosages, the most pronounced effect was observed at 0.02 wt.%. Relatively low dosages (0.02 wt.% and 0.04 wt.%) provided a clear improvement in the strength of the cement system, whereas the dosage of 0.10 wt.% resulted in the lowest performance among the modified compositions. The 0.02 wt.% dosage was found to be effective in enhancing the strength characteristics of the cement system and reducing water absorption, which supports its recommendation for industrial-scale implementation. This result confirms the high efficiency of the additive in improving the overall quality of concrete.

X-ray diffraction analysis was performed for unmodified cement samples and modified cement samples obtained 3 days after treatment. The modified cement specimen was prepared with an intensifier dosage of 0.02 wt.% and a water-to-cement ratio of  $w/c = 0.24$ . The XRD patterns of these samples are presented in Fig. 9 and 10.

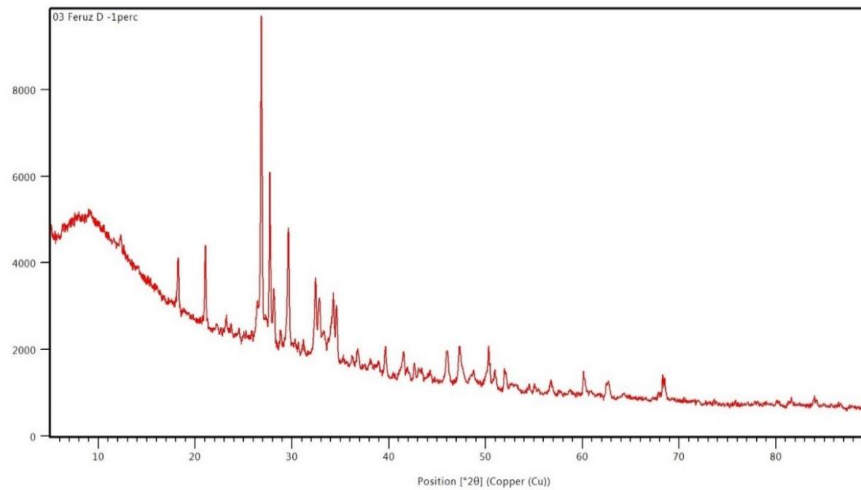


**Fig. 9.** X-ray diffraction (XRD) pattern of the control cement sample.

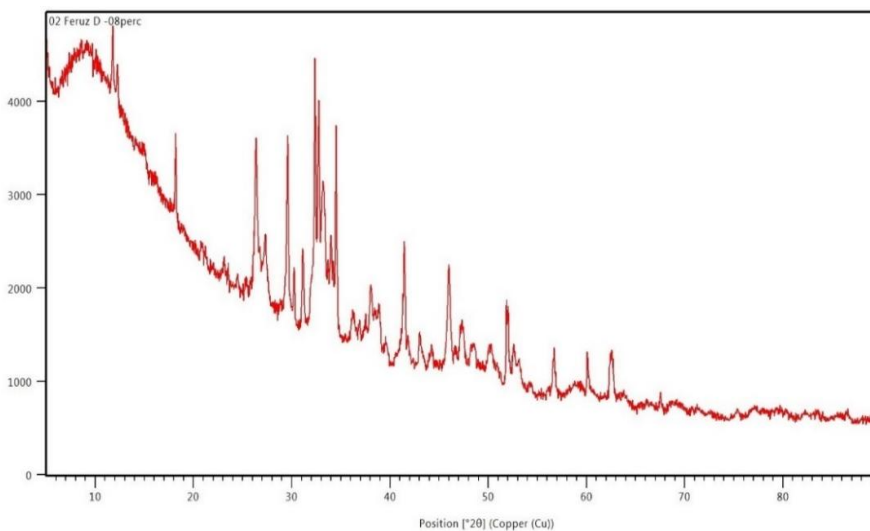


**Fig. 10.** X-ray diffraction (XRD) pattern of the modified cement.

As shown in Fig. 9, the XRD pattern of cement prior to hydration is characterized mainly by calcium silicate phases ( $C_2S$  and  $C_3S$ ), which exhibit high-intensity reflections within the  $30-33^\circ$   $2\theta$  range. The aluminates ( $C_3A$ ) and ferrite ( $C_4AF$ ) phases are also observed, with characteristic peaks in the  $40-45^\circ$   $2\theta$  region. Low-intensity absorbed regions may correspond to calcium oxide ( $CaO$ ) or calcium hydroxide ( $Ca(OH)_2$ ) phases. The XRD pattern in Figure 10 corresponds to cement cured for 3 days, i.e., a hydrated sample. A slight decrease in diffraction intensity of calcium silicate phases ( $C_2S$  and  $C_3S$ ) is observed, whereas the diffraction intensity of calcium hydroxide ( $Ca(OH)_2$ ) increases. This indicates the formation of calcium hydroxide and calcium silicate hydrate ( $C-S-H$ ) during cement hydration. The diffraction peaks of these phases appear mainly in the ranges of  $30-33^\circ$   $2\theta$  and  $40-45^\circ$   $2\theta$ . In addition, the presence of aluminates ( $C_3A$ ) and ferrite ( $C_4AF$ ) phases in the  $40-45^\circ$   $2\theta$  region is accompanied by calcium carbonate ( $CaCO_3$ ) signals in low-intensity regions between  $29.4^\circ$   $2\theta$  and  $48.5^\circ$   $2\theta$ , which may be associated with  $CO_2$  uptake from the atmosphere. These changes reflect phase transformations during hydration and the formation of phases that are critical for strength development.

One of the key functional roles of grinding intensifiers is to promote dispersion of the cement–aggregate mixture. Grinding intensifiers should improve the rheological behavior of cement-based



The derivatogram is presented in Fig. 11 and consists of two curves. Two endothermic effects were observed at 424.74°C and 691.52°C. In this temperature range, two endothermic peaks were also detected on the DTA curve at 424.74°C and 691.52°C. The endothermic peak at 691.52°C can be attributed to the thermal decomposition of the intensifier and/or bond rupture within the composite structure.

For FTIR analysis of cement stone containing the grinding intensifier, specimens with 0.02 wt.% additive dosage were used. The FTIR spectrum obtained from the tests is shown in Fig. 12.

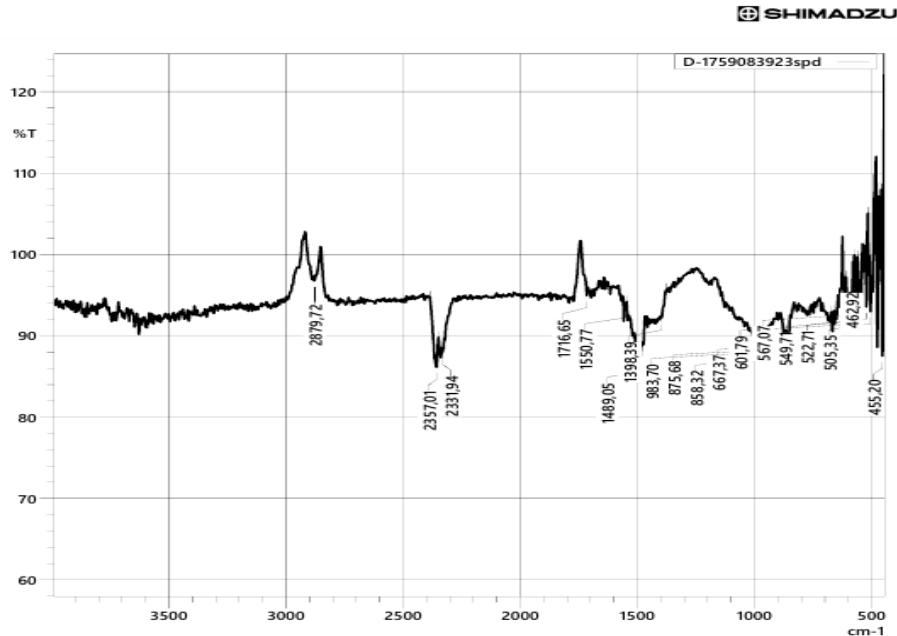


**Fig. 12.** FTIR spectrum of cement stone containing 0.02 wt.% grinding intensifier.

The absorption maximum in the 1400-1600  $\text{cm}^{-1}$  region, as well as the broad spectral band within 2357-2331  $\text{cm}^{-1}$ , indicate the presence of submicrocrystals of calcium hydrosilicates of the tobermorite group, the content of which is higher in the specimens containing the grinding intensifier than in the reference composition without additives. The high spectral resolution in these regions suggests a high degree of crystallinity of the above-mentioned calcium hydrosilicates formed in the presence of the intensifier. A narrow and well-resolved absorption band at 2879  $\text{cm}^{-1}$  is characteristic of hydroxyhydrosilicates of the honolite group. These results demonstrate that the incorporation of grinding intensifier additives into the cement composition improves the quality of the resulting concrete.

The hydrate phase composition of Portland cement-based concrete (PC400 D20) containing different grinding intensifier formulations was examined using electron microscopy.

As the calcium hydroxide content decreases, the likelihood of formation and persistence of polybasic calcium hydroaluminates is reduced. The hydration products formed during crystallization in the presence of fine grinding intensifiers fill pores and capillaries in the Portland cement stone, thereby densifying and strengthening its microstructure.

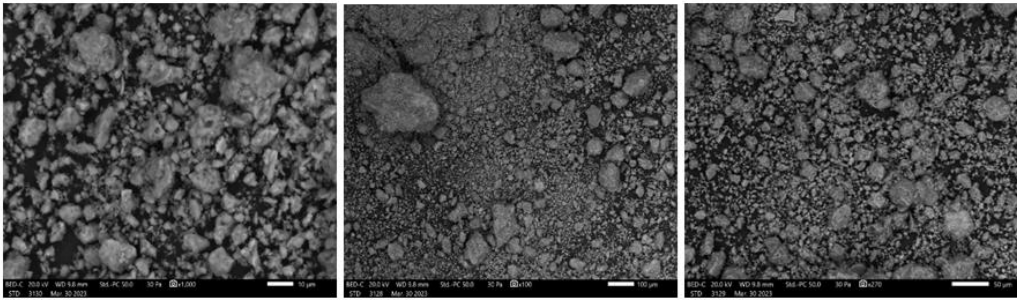


**Fig. 13.** Scanning electron microscopy (SEM) images of the concrete sample without additives.

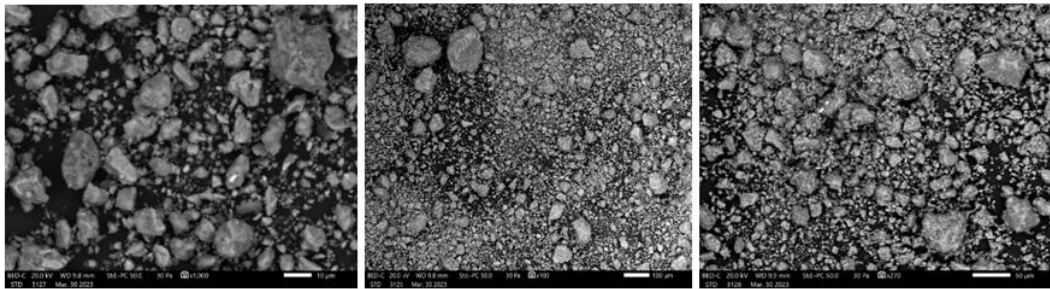


**Fig. 14.** Scanning electron microscopy (SEM) images of cement stone containing 0.02 wt.% grinding intensifier.

SEM micrographs of cement stone specimens containing the grinding intensifier show pore filling within the cement matrix, indicating a denser microstructure. In addition, the specimens with the intensifier exhibit a higher amount of calcium hydrosulfoaluminate phases (ettringite-type hydrates). An increased content of calcium hydrosulfoaluminate and the corresponding increase in the specific surface area of the hydrate phases – both in the bulk structure and in defect-prone regions of the spatial framework – contribute to material hardening.

The densification and strengthening of Portland cement compositions at early curing stages are associated with the growth and crystallization of gypsum and calcium hydrosulfoaluminate phases in the presence of the intensifier. The resulting fine-dispersed crystalline products form more readily, effectively sealing pores and capillaries in the hardened cement paste, thereby compacting and reinforcing its structure. The hydrate phase assemblage of cement stone prepared under standard consistency conditions using PC400 D20 cement with various intensifier compositions was examined by electron microscopy. Needle-like ettringite crystals were observed within the main gel-like matrix, filling available voids. New ettringite formations were also detected in free volumes. In specimens containing the intensifier, pores were found to be filled with both gypsum and calcium hydrosulfoaluminate. Overall, the increased concentration of calcium hydrosulfoaluminate and the higher specific surface area of the hydrated phases promote early-age densification and strengthening of the Portland cement microstructure.

#### 4.CONCLUSIONS

The efficiency of the proposed purification method for methyldiethanolamine (MDEA), a waste product generated during natural gas sweetening, was evaluated using FTIR spectroscopy. The results confirmed a high purity of the purified MDEA and demonstrated the high effectiveness of the proposed purification approach.

The optimal conditions for grinding intensifier synthesis were identified as a reaction temperature of 45°C, a reaction time of 6 h, and a component ratio of 1:9. The product obtained under these conditions exhibited high performance. The ninefold excess of MDEA relative to hydrolyzed

polyacrylonitrile (GI-PAN) in the initial mixture can be explained by the presence of intramolecular hydrogen bonds in the GI-PAN structure, which hinder the reaction of carboxyl groups with amines; weakening of these hydrogen bonds requires a strongly alkaline medium.

Particle size analysis of the modified cement showed that the particles exhibit a predominantly spherical morphology. The maximum laser diffraction value was 13.5%, the intensity reached 88%, and the dominant particle size was approximately 2  $\mu\text{m}$  (more than 53.5%). The fraction of particles in the 100-200  $\mu\text{m}$  range was 4.87%.

Differential thermal analysis indicated that the absence of endothermic effects and the low mass loss below 200°C correspond to a very low level of free water. The absence of exothermic effects up to 200°C suggests that the grinding intensifiers do not undergo chemical transformations within this temperature range and can be safely applied under thermal-moist curing conditions.

FTIR spectra and XRD patterns of modified cement showed a slight decrease in the diffraction intensity of calcium silicate phases ( $\text{C}_2\text{S}$  and  $\text{C}_3\text{S}$ ), accompanied by an increased diffraction intensity of calcium hydroxide ( $\text{Ca}(\text{OH})_2$ ), indicating the formation of calcium hydroxide and calcium silicate hydrate (C-S-H) during cement hydration. These changes reflect phase transformations in the cement system and the formation of phases contributing to strength development.

Electron microscopy confirmed that cement stone samples containing the grinding intensifier exhibit pore filling within the microstructure. In addition, a predominance of calcium hydrosulfoaluminate phases was observed. The increased concentration of calcium hydrosulfoaluminate and the corresponding increase in the specific surface area of hydrated phases – both in the bulk structure and in defect-prone regions – contribute to densification and strengthening of the cement stone.

## 5. ACKNOWLEDGEMENTS

The study was carried out within the framework of the research project AP26102705 “Development and Production of Cement Grinding Intensifiers Based on Local Raw Materials”, funded by the Science Committee of the Ministry of Science and Higher Education of the Republic of Kazakhstan

## REFERENCES

1. Scrivener K.L., John V.M., Gartner E.M. Eco-efficient cements: potential economically viable solutions for a low-CO<sub>2</sub> cement-based materials industry. *Cement and Concrete Research*. 2018. 114. P. 2 – 26. <https://doi.org/10.1016/j.cemconres.2018.03.015>
2. Juenger M.C.G., Snellings R., Bernal S.A. Supplementary cementitious materials: new sources, characterization, and performance insights. *Cement and Concrete Research*. 2019. 122. P. 257 – 273. <https://doi.org/10.1016/j.cemconres.2019.05.008>
3. Snellings R. Assessing, understanding and unlocking supplementary cementitious materials. *RILEM Technical Letters*. 2016. 1. P. 50 – 55. <https://doi.org/10.21809/rilemtechlett.2016.12>
4. Pan D., Li L., Tian X., Wu Y., Cheng N., Yu H. A review on lead slag generation, characteristics, and utilization. *Resources, Conservation and Recycling*. 2019. 146. P. 140 – 155. <https://doi.org/10.1016/j.resconrec.2019.03.036>
5. Gholizadeh A., Horckmans L., Snellings R., Peys A., Teck P., Maier J., Friedrich B., Klejnowska K. Use of Treated Non-Ferrous Metallurgical Slags as Supplementary Cementitious Materials in Cementitious Mixtures. *Applied Sciences*. 2021. 11 (9). P. 4028. <https://doi.org/10.3390/app11094028>
6. Sivakumar P.P., Matthys S., De Belie N., Gruyaert E. Reactivity Assessment of Modified Ferro Silicate Slag by R3 Method. *Applied Sciences*. 2021. 11 (1). P. 366. <https://doi.org/10.3390/app11010366>
7. Hallet V., Pedersen M.T., Lothenbach B., Winnefeld F., De Belie N., Pontikes Y. Hydration of blended cement with high volume iron-rich slag from non-ferrous metallurgy. *Cement and Concrete Research*. 2022. 151. P. 106624. <https://doi.org/10.1016/j.cemconres.2021.106624>

9. Sergeeva I.V., Botabaev N.E., Al'zhanova A.Zh., Ashirbaev Kh.A. Chemical and phase transitions in oxidized manganese ore in the presence of carbon. *Steel in Translation*. 2017. 47 (9). P. 605 – 609. <https://doi.org/10.3103/S0967091217090078>
10. Sarsenbayev B., Murtazaev S.-A., Salamanova M., Kuldeyev E., Saidumov M., Sarsenbayev N., Auyesbek S., Sauganova G., Abduova A. Utilization of Anthropogenic and Natural Waste to Produce Construction Raw Materials. *Sustainability*. 2025. 17 (7). P. 2791. <https://doi.org/10.3390/su17072791>
11. Auyesbek S., Sarsenbayev B., Lesovik V., Kolesnikova O., Begentayev M., Kuldeyev E., Tulaganov B., Sauganova G., Zhumayev Z. Studies on the Production of a Ground Silicate Composite Based on a Mineral Slag Binder with the Disposal of Industrial Waste. *Journal of Composites Science*. 2025. 9 (5). P. 225. <https://doi.org/10.3390/jcs9050225>
12. Zhanikulov N., Taimasov B., Shal A. Influence of industrial waste on the structure of environmentally friendly cement clinker. *Kompleksnoe Ispolzovanie Mineralnogo Syra = Complex Use of Mineral Resources*. 2022. 323 (4). P. 84 – 91. <https://doi.org/10.31643/2022/6445.44>
13. Ristavletov R.A., Baybolov K.S., Kopzhasarov B.T., Kambarov M.A., Imanaliev K.E., Ibraimbayeva G.B., Abshenov Kh.A., Kudabayev R.B. Effective multifunctional additives for concrete based on the wastes of the oil industry. *Structural Concrete*. 2019. 20 (6). P. 1–10. <https://doi.org/10.1002/suco.201700284>
14. Kolesnikov A.S., Zhanikulov N.N., Kuraev R.M. Thermodynamic modeling of the synthesis of the main minerals of cement clinker from technogenic raw materials. *Kompleksnoe Ispolzovanie Mineralnogo Syra = Complex Use of Mineral Resources*. 2021. 318 (3). P. 24 – 34. <https://doi.org/10.31643/2021/6445.25>
15. Auyesbek S.T., Sarsenbayev N.B., Sarsenbayev B.K., Khudyakova T.M., Aimenov Zh.T., Abdiramanova K.S., Aubakirova T.S., Sauganova G.R., Karshyga G.O., Nurbaeva F.K. Thermal insulating materials based on Magnesium-containing technogenic raw Materials. *Rasayan Journal of Chemistry*. 2023. 16 (1). P. 413 – 421. <https://doi.org/10.31788/RJC.2023.1618327>
16. Muratov B., Shapalov S., Syrlybekkyzy S., Volokitina I., Zhunisbekova D., Takibayeva G., Nurbaeva F., Aubakirova T., Nurshakhanova L., et al. Physico-Chemical Study of the Possibility of Utilization of Coal Ash by Processing as Secondary Raw Materials to Obtain a Composite Cement Clinker. *Journal of Composites Science*. 2023. 7 (6). P. 234. <https://doi.org/10.3390/jcs7060234>
17. Mishra R.K., Weibel M., Müller T., Heinz H., Flatt R.J. Energy-effective grinding of inorganic solids using organic additives. *Chimia*. 2017. 71 (7-8). P. 451 – 460. <https://doi.org/10.2533/chimia.2017.451>
18. Kuldeyev E., Begentayev M., Sarsenbayev B., Syrlybekkyzy S., Agabekova A., Bayamirova R., Togasheva A., Zholbassarova A., Koishina A., et al. Investigation of the Possibility of Utilizing Man-Made Waste to Produce Composite Binders. *Journal of Composites Science*. 2025. 9 (10). P. 531. <https://doi.org/10.3390/jcs9100531>
19. Marazzani B., Bürge C., Kurz C., Müller T. Dialkanolamines as additives for grinding of solids. 2015.
20. Zhanikulov N., Khudyakova T., Taimassov B., Sarsenbayev B., Dauletiarov M., Karshygayev R. Receiving Portland Cement from Technogenic Raw Materials of South Kazakhstan. *Eurasian Chemico-Technological Journal*. 2019. 21 (4). P. 333 – 340. <https://doi.org/10.18321/ectj890>
21. Sapargaliyeva B.O., Bychkov A.Yu., Alferyeva Ya.O., Syrlybekkyzy S., Altybaeva Zh.K., Nurshakhanova L.K., Seidaliyeva L.K., Suleimenova B.S., Zhidebayeva A.E., Zhanikulov N.N., Suleimenova T.N., Koshkarbayeva Sh.K., Suigenbayeva A.Zh. Thermodynamic modeling of the formation of the main minerals of cement clinker and zinc fumes in the processing of toxic technogenic waste of the metallurgical industry. *Rasayan Journal of Chemistry*. 2022. 15 (3). P. 2181 – 2187. <https://doi.org/10.31788/RJC.2022.1536230>

22. Amiraliyev B., Taimasov B., Potapova E., Sarsenbaev B., Begentayev M., Dauletiyarov M., Kuandykova A., Abdullin A., Ainabekov N., Auyesbek S. Heat Treatment of Clay Shales and Their Utilization as Active Mineral Additives for the Production of Composite Cements. *Journal of Composites Science*. 2025. 9 (6). P. 269. <https://doi.org/10.3390/jcs9060269>
23. Auyesbek S., Sarsenbayev N., Abduova A., Sarsenbayev B., Uderbayev S., Aimenov Z., Kenzhaliyeva G., Akishev U., Aubakirova T., Sauganova G., et al. Man-Made Raw Materials for the Production of Composite Silicate Materials Using Energy-Saving Technology. *Journal of Composites Science*. 2023. 7 (3). P. 124. <https://doi.org/10.3390/jcs7030124>
24. Kuandykova A., Taimasov B., Potapova E., Sarsenbaev B., Begentayev M., Kuldeyev E., Dauletiyarov M., Zhanikulov N., Amiraliyev B., et al. Production of Composite Cement Clinker Based on Industrial Waste. *Journal of Composites Science*. 2024. 8 (7). P. 257. <https://doi.org/10.3390/jcs8070257>
25. Ismailov A.A., Baybolov K.S., Ristavletov R.A., Kopzhasarov B.T., Kambarov M.A., Ussipbaev U.A., Kudabayev R.B., Mominova S.M. Effect of Cost-Effective Alkaline Additives on the Hydration of Slag-Cement Mixtures. *Journal of Advanced Concrete Technology*. 2018. 16 (9). P. 429 – 440. <https://doi.org/10.3151/jact.16.429>
26. Ma S., Li W., Zhang S., Hu Y., Shen X. Study on the hydration and microstructure of Portland cement containing diethanol-isopropanolamine. *Cement and Concrete Research*. 2015. 67. P. 122 – 130. <https://doi.org/10.1016/j.cemconres.2014.09.002>
27. Xu Z., Li W., Sun J., Hu Y., Xu K., Ma S., Shen X. Research on cement hydration and hardening with different alkanolamines. *Construction and Building Materials*. 2017. 141. P. 296 – 306. <https://doi.org/10.1016/j.conbuildmat.2017.03.010>
28. Khudyakova T.M., Kenzhibayeva G.S., Kutzhanova A.N., Iztleuov G.M., Zhanikulov N.N., Kolesnikova O.G., Mynbaeva E. Optimization of Raw Material Mixes in Studying Mixed Cements and Their Physicomechanical Properties. *Refractories and Industrial Ceramics*. 2019. 60 (1). P. 76 – 81. <https://doi.org/10.1007/s11148-019-00312-2>
29. Huang H., Li X., Avet F., Hanpongpun W., Scrivener K. Strength-promoting mechanism of alkanolamines on limestone-calcined clay cement and the role of sulfate. *Cement and Concrete Research*. 2021. 147. P. 106527. <https://doi.org/10.1016/j.cemconres.2021.106527>
30. Khudyakova T.M., Kolesnikova O.G., Zhanikulov N.N., Botabaev N.E., Kenzhibayeva G.S., Iztleuov G.M., Suigenbaeva A.Z., Kutzhanova A.N., Ashirbaev H.A., Kolesnikova V.A. Low-base cement, problems and advantages of its use. *Refractories and Industrial Ceramics*. 2021. 62 (1). P. 3 – 9. <https://doi.org/10.17073/1683-4518-2021-7-3-9>
31. Zou F., Tan H., He X., Ma B., Deng X., Zhang T., Mei J., Liu X., Qi H. Effect of triisopropanolamine on compressive strength and hydration of steaming-cured cement-fly ash paste. *Construction and Building Materials*. 2018. 192. P. 836 – 845. <https://doi.org/10.1016/j.conbuildmat.2018.10.142>

## INFORMATION ABOUT THE AUTHORS

**Ristavletov R.A.**, e-mail: rar\_1967@mail.ru, ORCID: <https://orcid.org/0000-0001-7106-6611>, SCOPUS: <https://www.scopus.com/authid/detail.uri?authorId=57203588844>, South-Kazakhstan University named after M. Auezov, Department “Construction Materials and Expertise in Construction”, Candidate of Engineering sciences (PhD), Associate Professor

**Auyesbekova M.A.**, e-mail: Maral\_5@mail.ru, ORCID: <https://orcid.org/0009-0008-0577-6154>, South-Kazakhstan University named after M. Auezov, Department “Construction Materials and Expertise in Construction”, Doctoral Student

**Karimov M.U.**, e-mail: masudkarimov27@gmail.com, ORCID: <https://orcid.org/0000-0001-5063-0914>, SCOPUS: <https://www.scopus.com/authid/detail.uri?authorId=57255641600>, Tashkent Research Institute of Chemical Technology, Doctor of Science (Advanced Doctor), Associate Professor

**Kambarov M.A.**, e-mail: medet\_2030@mail.ru, ORCID: <https://orcid.org/0000-0001-6397-1451>, SCOPUS: <https://www.scopus.com/authid/detail.uri?authorId=57203941118>, South-Kazakhstan University named after M. Auezov, Department “Construction Materials and Expertise in Construction”, Candidate of Engineering sciences (PhD), Associate Professor

**Kasimova G.A.**, e-mail: guzal.kasimova.62@mail.ru, ORCID: <https://orcid.org/0000-0001-5646-3109>, SCOPUS: <https://www.scopus.com/authid/detail.uri?authorId=57610238800>, Tashkent Institute of Architecture and Civil Engineering, Candidate of Engineering sciences (PhD), Associate Professor

**Kudabayev R.B.**, e-mail: kudabaev\_81@mail.ru, ORCID: <https://orcid.org/0000-0003-3482-8423>, SCOPUS: <https://www.scopus.com/authid/detail.uri?authorId=57195780947>, South-Kazakhstan University named after M. Auezov, Candidate of Engineering Sciences (Ph.D.)

**Bektursunova A.K.**, e-mail: Bektursunova7979@mail.ru, ORCID: <https://orcid.org/0000-0001-5514-5870> , SCOPUS: <https://www.scopus.com/authid/detail.uri?authorId=57193453995>, M. Auezov South Kazakhstan University, Department of Technology and Design of Textile Materials, Doctor of Philosophy (Advanced Doctor), Senior Lecturer

**Artykova Zh.K.**, e-mail: articova@mail.ru, ORCID: <https://orcid.org/0000-0002-6466-6317>, SCOPUS: <https://www.scopus.com/authid/detail.uri?authorId=57212768251>, South-Kazakhstan University named after M. Auezov, Candidate of Engineering Sciences (Ph.D.)